AgriEngineering

MDPI

Article

Operating Point Control System in Single-Phase Motor Pump Sets Used in Irrigation Systems: Development and Evaluation

Angelo Tiago Azevedo [1], Marinaldo Ferreira Pinto [2], Marcus Vinicius Morais Oliveira [2], Alexandre de Melo Pereira [3] and Daniel Fonseca de Carvalho [2,*]

[1] Department of Soil Science, Luiz de Queiroz College of Agriculture, University of São Paulo (ESALQ/USP), Av. Pádua Dias, 11, Piracicaba 13418-900, SP, Brazil; azevedo_angelo@usp.br
[2] Department of Engineering, Federal Rural University of Rio de Janeiro (UFRRJ), BR-465, Km 7, Seropédica 23897-000, RJ, Brazil; marinaldo@ufrrj.br (M.F.P.); marcus.oliveira@ufrrj.br (M.V.M.O.)
[3] Department of Architecture and Urbanism, Federal Rural University of Rio de Janeiro (UFRRJ), BR-465, Km 7, Seropédica 23897-000, RJ, Brazil; amelopereira@ufrrj.br
* Correspondence: carvalho@ufrrj.br; Tel.: +55-(21)-98787-7262

Abstract

Fixed irrigation systems often experience uneven water pressure across different sections, making it challenging to irrigate all areas efficiently without wasting energy. This issue is particularly evident when using low-power, single-phase motors. To address this, we created a load controller that fine-tunes how these motors work in irrigation systems with changing needs. Our load controller uses a MOC-TRIAC circuit and an Arduino Nano to adjust motor power. Furthermore, we developed a smartphone app that connects via Bluetooth, allowing users to conveniently set the motor power as needed. We tested it on two 1 hp motor pumps, using valves, a flow meter, and pressure gauges to simulate different conditions. By adjusting the "firing angle" of the motor, we were able to change the water pressure by up to 80% while maintaining the flow rate the same. This resulted in energy savings up to 70% and reduced current consumption by 50%. The only limitation occurred at very high-power reductions (75%) and low flow rates (below 3 m^3 h^{-1}), where motor overheating was observed. Overall, our load controller presents a promising solution to save energy in irrigation systems by precisely matching motor power to the system's needs.

Keywords: instrumentation; irrigation; control system; energy efficiency; irrigation systems; single-phase control

Academic Editor: Giovanni Rallo

Received: 11 July 2025
Revised: 2 September 2025
Accepted: 5 September 2025
Published: 15 September 2025

Citation: Azevedo, A.T.; Pinto, M.F.; Oliveira, M.V.M.; Pereira, A.d.M.; Carvalho, D.F.d. Operating Point Control System in Single-Phase Motor Pump Sets Used in Irrigation Systems: Development and Evaluation. *AgriEngineering* **2025**, *7*, 298. https://doi.org/10.3390/agriengineering7090298

1. Introduction

Energy consumption on rural properties is largely due to irrigation systems, especially pumping systems. Therefore, several studies have been developed aimed at reducing energy consumption through various actions, such as strategies to reduce water and energy consumption by choosing more efficient irrigation systems with lower pressure requirements, or through management strategies and the use of intelligent systems such as machine learning and IoT [1,2], predictive control systems using mathematical models and artificial intelligence to optimize irrigation and energy consumption [3], and control of the pump operating point through devices such as frequency inverters [4,5].

Pressurized irrigation systems require different types of hydraulic power throughout irrigation, given the sectorization and heterogeneity of the agricultural environment. Thus, pumping systems are often designed considering the scenario of maximum demand to meet all irrigation subunits [1–3].

A significant portion of irrigation systems uses motor pump sets with electric motors, and the operating point is adjusted by using valves with partial closure, which is a dissipative method [4,5]. Although technically feasible, this method increases energy consumption as the excess hydraulic energy generated by the pump is converted into head loss, which has no practical utility [6]. To address this, frequency inverters have been used to reduce energy consumption. These devices modify the electrical grid frequency, consequently adjusting motor speed and hydraulic power according to the irrigation system's demand or the requirements of irrigation subunits [6,7].

Electronic devices, such as inverters, allow the use of pumps in a wider operational range, helping to reduce electricity consumption, wear on system components, and performing ramp starts, which generate fewer disturbances in the local electrical system, avoiding unnecessary current peaks. However, although efficient and versatile, frequency inverters have a high acquisition cost and require specialized labor for programming and repair, often making them unfeasible in small pressurized systems [1]. Moreover, for single-phase motors, control methods cannot be applied analogously due to their distinct torque-speed behavior under variable-frequency supply compared to three-phase motors. [7].

In projects where the required power is less than 12.5 hp, the use of single-phase motors is common due to the lower acquisition cost, which according to [8], is lower than three-phase motors. Moreover, electrification in many rural properties can be found in a single-phase system [9]. The rotation of single-phase motors can be controlled by electronic devices, such as Triode for Alternating Current (TRIAC) [10,11]. These devices enable voltage control applied to the motor stator through optocouplers and microcontrollers. The voltage regulation is achieved by adjusting the TRIAC firing angle, which modifies the electrical power supplied to the motor and consequently its rotational speed [12]. According to [13], this speed control technique can provide energy savings while offering simplicity, reliability, and low acquisition cost.

Despite its advantages, firing angle control may reduce the power factor due to the introduction of voltage harmonics and increased stator current harmonics [14]. As noted by the authors, when torque is reduced, efficiency gains and loss reduction can be achieved, meaning the system's efficiency depends on the motor's operating conditions. Within an operational range that does not compromise motor electrical performance (considering the control technique's limitations), TRIAC-based voltage regulation enables pump load control for automated local or remote pressure adjustment in irrigation subunits via IoT tools, while offering potential electrical energy savings [15].

Within an operational range that does not compromise motor electrical performance (considering the control technique's limitations), TRIAC-based voltage regulation enables pump load control for automated local or remote pressure adjustment in irrigation subunits via IoT tools, while offering potential electrical energy savings. According to [13,14], system automation can improve water and energy application efficiency by enabling strategic irrigation scheduling. When combined with reduced water application volumes, this approach further lowers energy costs [12,16].

The prevalence of single-phase motors is a key factor in many agricultural contexts, particularly on small and medium-sized farms, where the power supply is often limited. While motor pump sets are essential for irrigation in these scenarios, the high cost and technical complexity of solutions like Variable Frequency Drives (VFDs) can be prohibitive. In this regard, a load control circuit based on a TRIAC presents a compelling alternative. This approach is not only cost-effective but also features a simpler implementation and reduced circuit complexity compared to VFDs. While the principles of TRIAC firing angle control have been explored in the previous literature, the novelty and main contribution of this work lie in the development of a low-cost electronic load controller integrated

with a user-friendly Bluetooth smartphone interface. This specific combination provides a highly accessible and economically viable solution, bridging the gap between fundamental control techniques and practical, real-world applications tailored for small-scale operations. This distinctive approach enhances the operational efficiency of motor pump sets while providing a platform for easy control and monitoring, which is a key advantage over similar devices or control methods available today [17,18].

In this context, the present study developed a load controller that adjusts the operating point of single-phase motor pump sets, using a more accessible technological platform with the same reliability as commercial models, while maintaining the operational range and energy savings. This study provides a practical and robust contribution to technological innovation in agriculture by directly addressing the problem of energy consumption in irrigation systems, with relevance for applications in small-scale agricultural contexts. By promoting the efficient use of water and energy, this work aligns directly with the United Nations' Sustainable Development Goals (SDGs), particularly SDG 6 (Clean Water and Sanitation), by optimizing water consumption, and SDG 7 (Affordable and Clean Energy), by reducing the energy expenditure of pumping.

2. Materials and Methods

2.1. Review of Control System Energy

The scientific literature has consistently explored the optimization of pumping systems to improve energy efficiency. Several studies have focused on load control solutions for single-phase motors, a particularly relevant challenge in low-power applications such as irrigation. Within this context, control systems based on MOC-TRIAC circuits have proven to be an effective and low-cost approach for power modulation. Table 1 presents a summary of key works in this area, highlighting the methodologies, technologies employed, and the results achieved in energy control systems using electronic drives.

Table 1. List of Papers about AC control motors with Moc-Triac systems.

Experiment Title	Number of Phases	Maximum Power (W)	Author
Implementation of AC-AC Volage Controller for Reduce Transient Current at Three Phase Induction Motor	3	2200	[14]
Speed Control of Single Phase Induction Motor using TRIAC and Bluetooth Device	1	500	[17]
Triac Speed Control of Three-Phase Induction Motor with Phase-Locked Loop Regulation	3	2200	[18]
Investigations on TRIAC Based Speed Controller for a Single-Phase Induction Motor Ceiling Fans	1	50	[19]
Modelling and test validation of high speed universal motors fed via a Triac	1	1250	[20]
Triac Based Novel Single Phase Step-Down Cycloconverter with Reduced THDs for Variable Speed Applications	1	1200	[21]
Assessment of Phase Control and Time-Proportional Control Schemes for TRIAC Applications	1	200	[22]

2.2. Architecture of System

The architecture of the proposed control system was designed to allow the precise adjustment of the power supplied to the motor, adapting it to the dynamic needs of the

irrigation system, specifically for single-phase motors with power up to 746 W (1 hp) and Bluetooth communication interface via mobile for data transmission. The solution is based on a microcontrolled processing center, which acts as the decision and control core. This core manages the modulation of primary energy through control relays and the MOC-TRIAC assembly, which operates as an electronic drive system for the motor load. The energy processing is regulated by an algorithm that uses zero-cross detection to synchronize the firing, allowing for the adjustment of the TRIAC's conduction angle. The adjustment of the system's operating point is performed in real-time, using feedback provided by the user as a basis, which ensures flexibility and adaptability in the field (Figure 1).

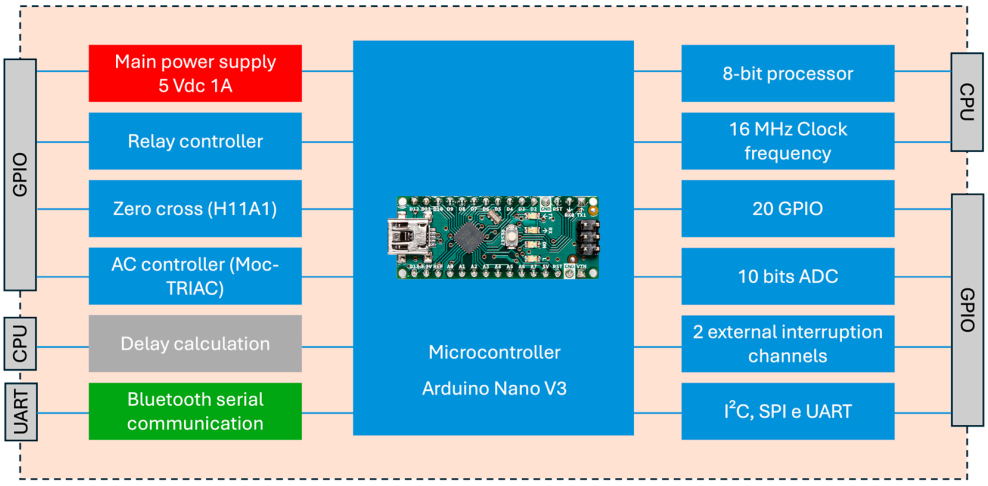

Figure 1. Electronic processing module.

The system architecture incorporates interfaces designed for seamless integration with the experimental module (Figure 2), thereby offering researchers a high degree of project flexibility and enabling versatile data acquisition. This inherent versatility allows the system to be adapted for controlling a variety of motor-pump types, including centrifugal, peripheral, multistage, and submersible models. The hardware's data acquisition capabilities feature a serial communication interface (UART), alongside multiple analog input channels and digital outputs (GPIOs), which facilitates the comprehensive monitoring of operational variables and precise actuation within the experimental setup.

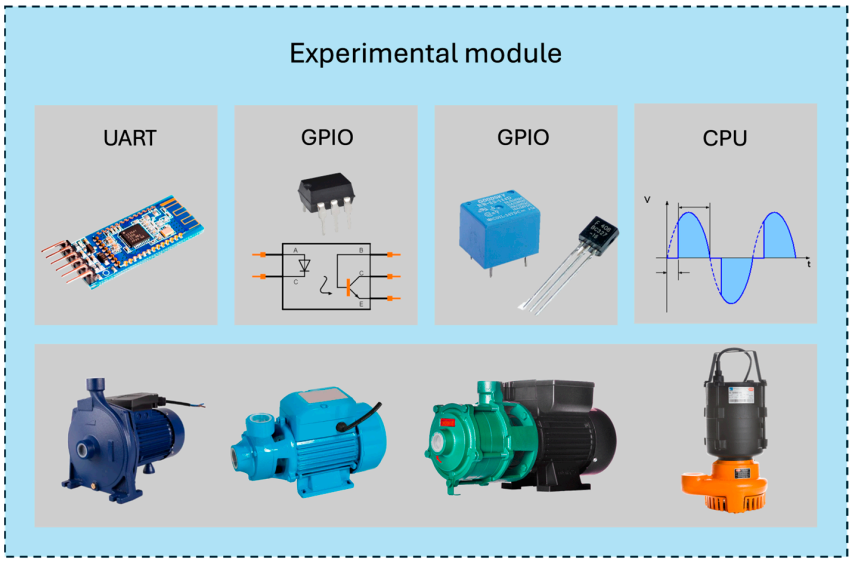

Figure 2. Experimental module.

2.3. Development of the Controller

The developed load controller was modeled using the KiCad version 9.0.1 software from Electronic Design Automation—open-source (EDA) [23], integrating a dimension of 9 × 11 cm, and built on a single-sided copper-clad phenolic board (Figure 1). It was programmed in C++ language through the Arduino integrated development environment. Its operating center was the Arduino Nano prototyping platform, which features an ATmega328p processor operating at a nominal frequency of 16 MHz [24]. The user interface was performed using a communication system comprising an HM-10 Bluetooth module, which operates with a CC2541 chipset equipped with a −94 dBm receiver at a speed of 1 Mbps [25]. The electronic components used, electrical connections and the relationships between the components are presented in Figures 3 and 4.

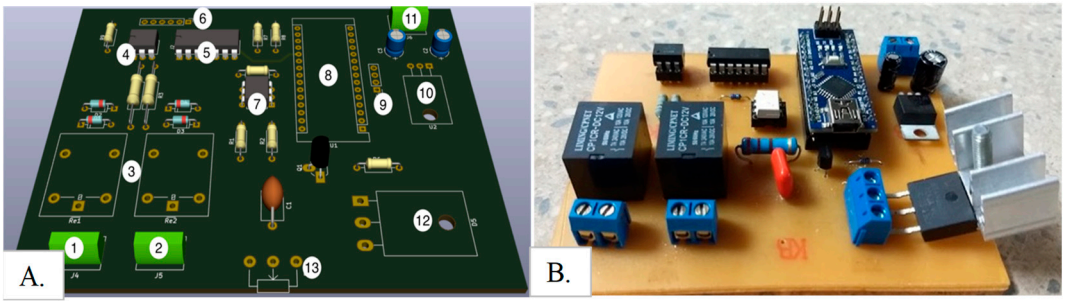

Figure 3. Load controller: (**A**) 3D digital version: (1—AC power input, 2—AC output, 3—control relays, 4—H11A1; 5—CD4093; 6—connection for HM-10 Bluetooth module; 7—MOC3020; 8—Arduino Nano version 3.0; 9—I2C output; 10 – Voltage regulator LM7805; 11 – DC Jack connector; 12 – Triac BTA41600; 13 – Potentiometer for analog control); (**B**) Built load controller.

The power variation by the controller is performed through the MOC3020 optical coupler, which, upon receiving a pulse (Figure 5), allows the passage of low-power electrical current, responsible for saturating the active zone of the BTA41600 TRIAC, initiating the conduction of high-power electricity until the polarity is reversed. This point at which the polarity is reversed is defined as the zero crossing [26].

The zero-crossing point is identified by the H11A1 phototransistor, responsible for emitting a pulse at each polarity inversion of the AC mains. These pulses are read by the microcontroller's digital pin using the Attach Interrupt function, in Rising mode, which triggers the internal timer according to the desired cutoff interval. After this time, the microcontroller emits a pulse to activate energy conduction through the MOC-TRIAC assembly (Figure 4). The algorithm flowchart embedded in the load controller is shown in Figure 6.

The t1 delay time is a crucial parameter in the TRIAC-based control algorithm, defining the interval between the zero-crossing detection of the sinusoidal voltage wave and the activation of the MOC-TRIAC assembly. This delay corresponds directly to the firing angle (α), where $\alpha = (t1/T\_half) \times 180°$, with T_half representing the half-cycle time of the AC supply (approximately 8.33 ms for a 60 Hz frequency). By increasing the value of t1, a larger portion of the sinusoidal wave is suppressed, subsequently reducing the effective voltage supplied to the motor. This mechanism allows for precise modulation of the motor's power and, consequently, its speed. The control system interprets a user-defined cutoff percentage (ranging from 0% to 100%) and translates this into a corresponding t1 delay, which spans from 0 ms (no cutoff) to 8.33 ms (full half-cycle cutoff). This direct linear relationship provides a predictable and effective means of regulating the motor's operational output [27].

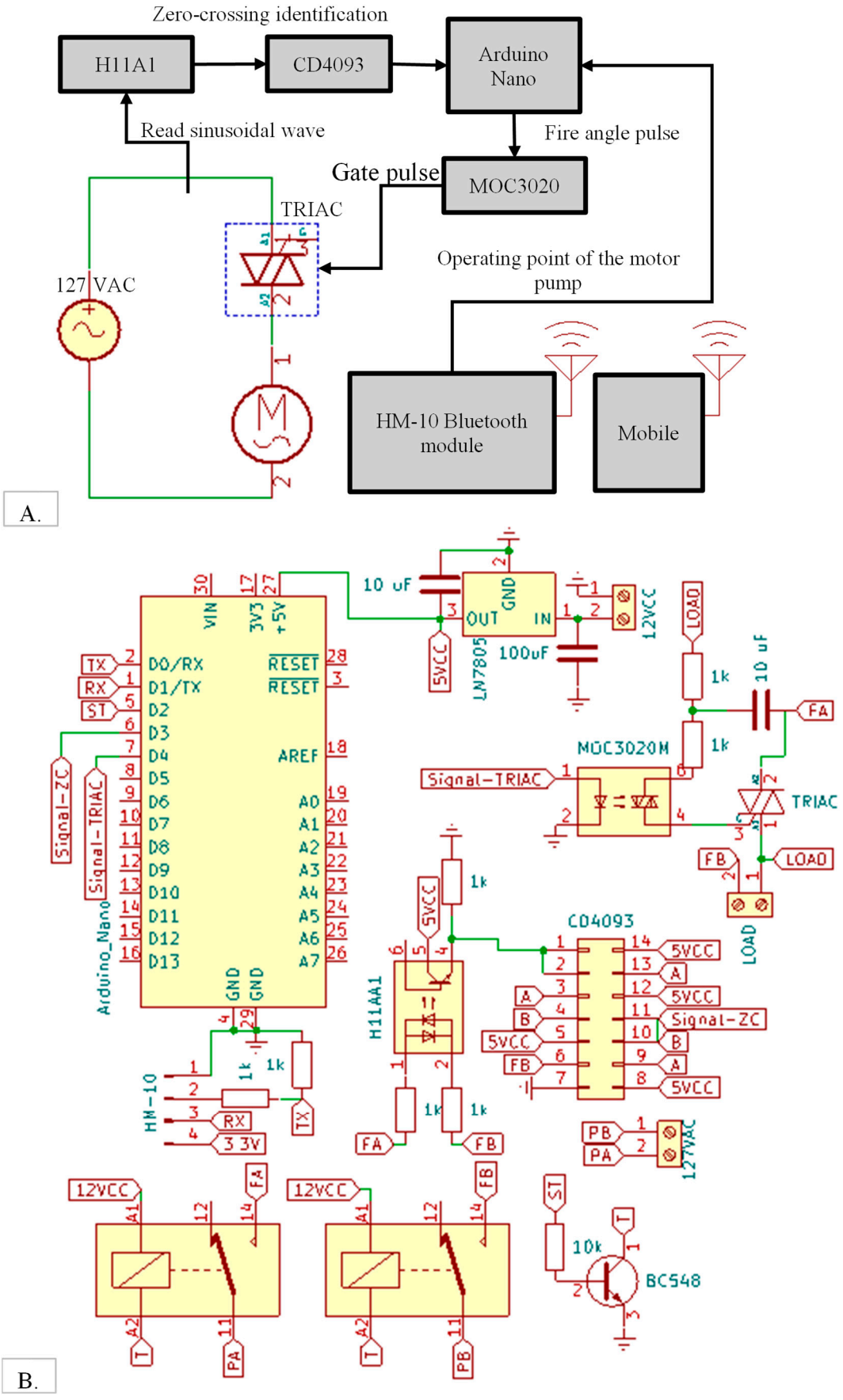

Figure 4. (**A**) Block diagram; (**B**) Electrical diagram.

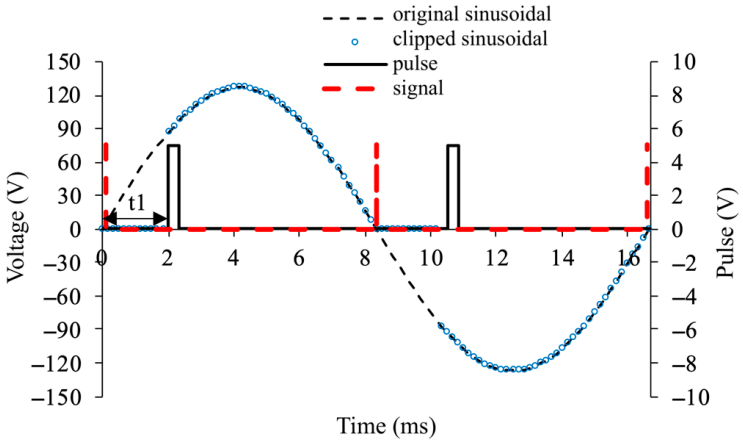

Figure 5. Representation of the sinusoidal supply (original), cut pulse, sinusoidal with cut, and zero-crossing signal.

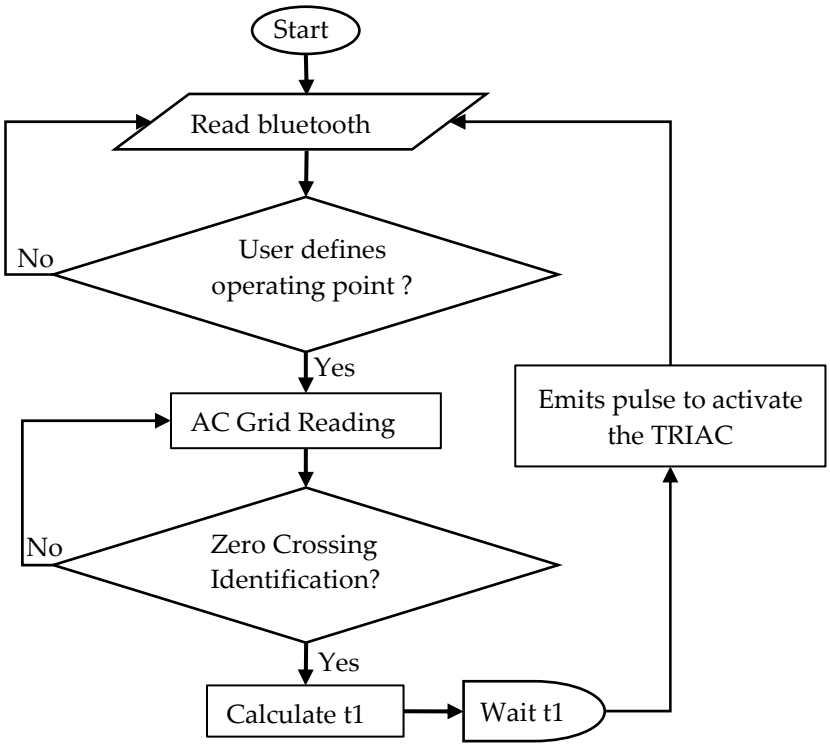

Figure 6. Flowchart of the algorithm embedded in the load controller.

2.4. Communication Interface

Device control is carried out via a smartphone using the "Serial Bluetooth Terminal" software version 1.49 (Figure 7), which is freely distributed on the Google Play platform. The software was used to send a message to the controller informing the operating point of the motor pump, allowing remote activation and reducing the presence of physical buttons on the controller.

The communication between the user application and the controller is established via Bluetooth, with messages sent directly to the device's serial port. The protocol allows the user to select the desired control mode: either by defining a target operating point (pressure and flow) or by specifying a direct cutoff percentage. For the first option, the user sends two distinct commands to set the target pressure in meters of water column (mwc) and the flow rate in cubic meters per hour (m^3h^{-1}), using the formats "P:xx and Q:yy", respectively. Alternatively, the user can choose to bypass the pressure/flow control and send a direct

command to set a specific cutoff percentage between 0% and 100% using the format "C:zz". The controller is programmed to interpret these commands to adjust the TRIAC's firing angle, accordingly, modulating the power supplied to the motor. To ensure reliability, the system includes a basic validation scheme: upon receiving a valid command, the controller sends an acknowledgment message back to the application, confirming proper reception in environments prone to interference or signal loss.

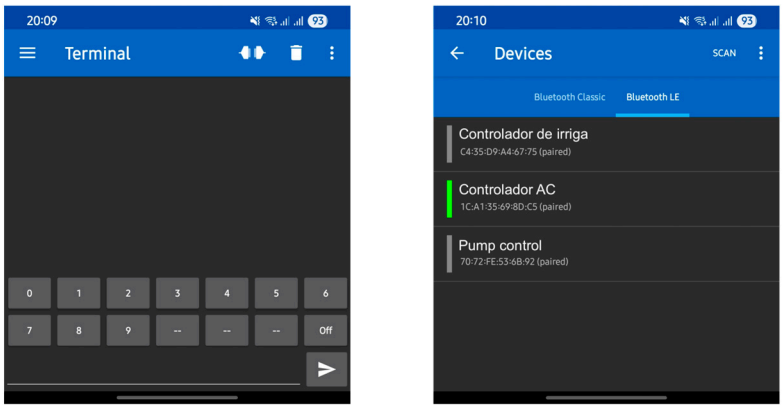

Figure 7. Communication software forms: (**A**) Control interface through the terminal in the communication application; (**B**) Device selection screen.

2.5. Experimental Tests: Electrical and Hydraulics Performance of Motor Pumps Under Firing Angle Control

To evaluate the operation of the firing angle in cutting the sinusoidal wave, a resistive load of 180 Ω was used, powered by the controller configured with 4 cutting ranges (20%, 50%, 75%, and 90%) and full conduction. The verification of the cutting levels was analyzed using the Tektronix 2205 oscilloscope, which has an AC voltage limit of 80 V. Therefore, a 127 V AC to 12 V AC transformer was used to lower the voltage level.

Two models of motor pumps with a nominal power of 1 hp were used to evaluate the technical feasibility of the operating point control (Table 2). Moreover, the performance curves under different flow rates and manometric head were determined and adjusted using the motor pump test bench (Figure 8).

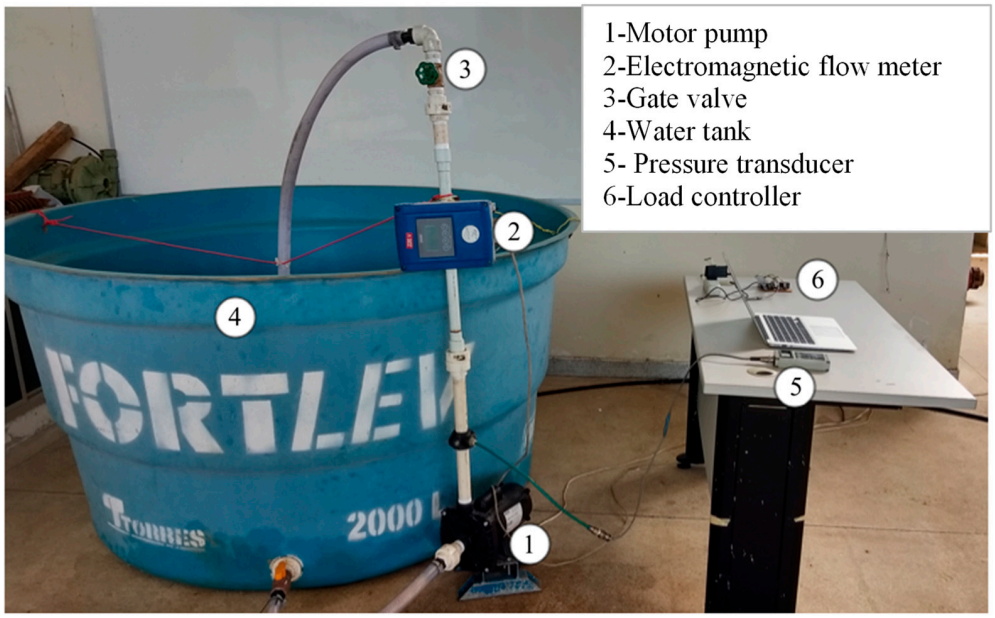

Figure 8. Test bench for evaluating the performance of the load controller and pumps.

Table 2. Characteristic data of the motor pump sets used in the test.

Model	Diameter	Rotation	IP	Voltage	Current	Efficiency	Qmax	Pmax
	Inch	RPM	-	V	A	%	$m^3\ h^{-1}$	mwc
A	1	3500	21	127	5	31	7	26
B	1	3500	21	127	5.2	69	11.6	29

RPM: revolutions per minute; IP: ingress protection; Qmax: maximum flow rate; Pmax: maximum pressure head.

The routine for determining the performance curves of the motor pumps consisted of configuring 7 cutoff levels (0; 15, 30, 45, 60, 75, and 90%) of the sinusoidal wave, followed by adjusting the manometric height, which was varied at 7 levels (35, 30, 25, 20, 15, 10, and 5 mwc). This variation was carried out through localized head loss, inserted into the system using a gate valve attached to the pump outlet. During the tests, for each of the pumps, 7 operating points (flow rate versus pressure) were tested for each of the proposed cuts, where for each pressure variation, a minimum period of 5 min was expected to ensure stability in the readings. Thus, each pump set underwent a total testing period of four hours and no repetitions of the readings are carried out.

The measurement of pressure and flow rate was carried out, respectively, using a pressure transducer MSI 300-250-P-3-N (maximum pressure of 70 mwa, with an uncertainty of 0.1 mwa) and the electromagnetic flow meter Krohne Conaut, OPTILUX KC 1000C/6 IFC 100C (measurement capacity of up to 10 $m^3\ h^{-1}$, with an uncertainty of 0.5%). After data collection, the construction of the characteristic curves of each motor pump set for the respective cut levels followed, which, when integrated, form a response surface.

Concurrently with the flow and pressure readings, the energy parameters were measured using a Westinghouse Type PG 191 industrial network analyzer, providing values for current, voltage, power, and power factor. It should be mentioned that these readings were manually performed.

To assess the effectiveness of the controller in the motor pump operation, the active power (Equation (1)), hydraulic power (Equation (2)), and total efficiency of the motor-pump set (Equation (3)) were calculated.

$$Pot_A = U \times I \times \cos(\varphi) \quad (1)$$

$$Pot_H = \gamma \times P \times Q \quad (2)$$

$$n_T = \frac{Pot_H}{Pot_A} \quad (3)$$

where

Pot_A—Active power (W);
U—Voltage (V);
I—Current (A);
$\cos(\varphi)$—Power factor;
Pot_H—Hydraulic power (W);
γ—Specific weight of water (N m^{-3});
P—Pressure (mwc);
Q—Flow rate ($m^3\ s^{-1}$);
n_T—Total efficiency (%).

Finally, by integrating the flow rate versus pressure curves, the useful operating range of the motor pumps was obtained.

To further understand the relationships between the system's input and output variables, the Response Surface Methodology (RSM) was adopted. This approach was con-

ducted in the R statistical environment, utilizing the "rsm" package for fitting second-order polynomial models that describe the behavior of the response variables. Specifically, two distinct quadratic regression models were generated using the least squares method. The first model aimed at estimating the flow rate as the response variable, with the sinusoidal cutoff (or firing angle control) and outlet pressure serving as the independent predictor factors. Concurrently, the second model was developed to estimate the efficiency, utilizing hydraulic power and the sinusoidal cutoff (or firing angle control) as its independent predictor factors. Subsequently, the "plotly and ggplot2" packages were employed for constructing interactive three-dimensional response surfaces, aiming to visually map the behavior of these critical performance variables (flow rate and efficiency, respectively) as a function of their controllable predictor factors. This methodology facilitates the identification of optimal operational conditions and the comprehension of multifactorial interactions within the evaluated system [28,29].

3. Results

3.1. Electrical Performance of Motors Under Firing Angle Control

The controller output signal after cutting the sinusoidal wave is shown in Figure 9. It can be observed that the controller was effective in cutting the sinusoidal wave by varying the TRIAC trigger angle, for all evaluated firing angles, allowing the variation in the average voltage supplying the load and, consequently, the power control.

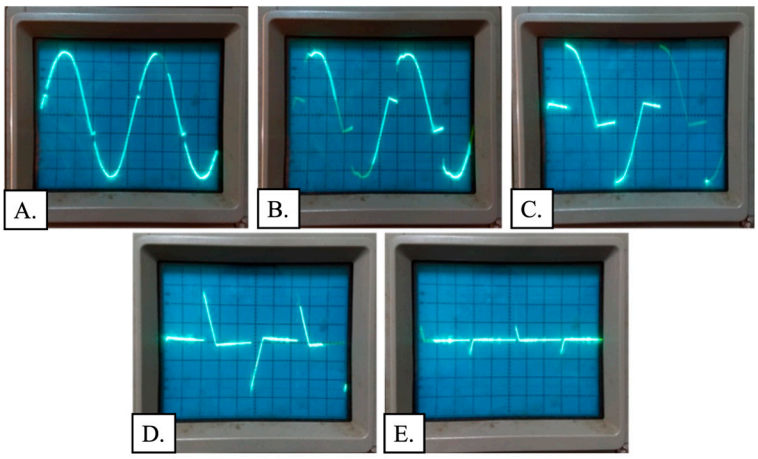

Figure 9. Voltage behavior after the cuts performed in the sinusoidal wave by the load controller at levels of 0% (**A**), 20% (**B**), 50% (**C**), 75% (**D**), and 90% (**E**).

The TRIAC allowed current conduction even after passing through the zero-voltage point (Figure 10B). This can be explained by the slight delay in obtaining the signal corresponding to Zero Cross and its conversion into a square wave for reception by the microcontroller. However, for cuts greater than 50% (Figure 9C–E), d the voltage stabilization can be observed around zero before the TRIAC is triggered. It is noteworthy that as the activation signal always has the same delay and is performed at the same point, it did not cause any problem to the operation of the controller or motor pump. The effective reduction in the average supply voltage to the motor, achieved through the TRIAC's firing angle control, directly influenced the motor's operating characteristics. This resulted in a weakening of the motor's magnetic field, leading to a decrease in its rotational speed. Consequently, the pump's operating point was altered, generating a series of new characteristic curves across the tested voltage reduction levels. These changes in the operating point were directly observed in the power consumption and flow rate data, indicating the controller's effectiveness in modulating the hydraulic performance of the motor-pump sets.

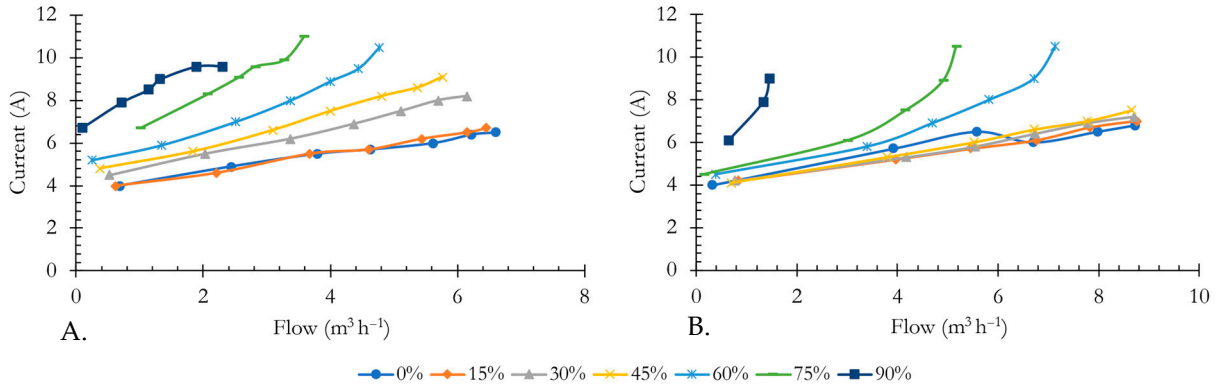

Figure 10. Current consumption curves of the motor pumps for different cuts of the sinusoidal wave (0; 15; 30; 45; 60, 75, and 90%) performed by the power controller: (**A**) Pump A; (**B**) Pump B.

In general, the motor-pump assemblies show a proportional relationship between the increase in flow rate and current, where the increase in load on the motor shaft requires greater energy consumption (Figure 10).

Figure 11 illustrates the variation in the active power of the motor-pump systems as a function of the flow rate and the percentage cuts in the waveform of the supply voltage. This magnitude shows the ability of the circuit to produce output throughout a certain period during the test. For both motor-pump assemblies, a reduction in active power is evident as the percentage of waveform cuts in the supply voltage increases, confirming a decrease in the circuit's output capacity.

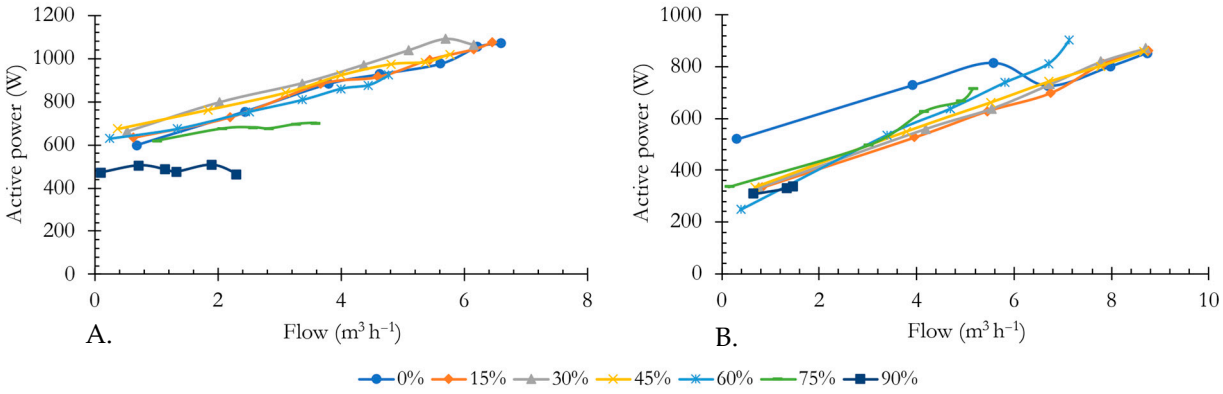

Figure 11. Variation in active power of the motor pumps as a function of flow rate and for different percentage cuts in the sinusoidal waveform: (**A**) Pump A; (**B**) Pump B.

Figure 12 shows the power factor (PF) as a function of flow rate for the pumps and waveform cuts. For the same operating ranges, it can be observed that Pump A (Figure 12A) presents a better PF than Pump B (Figure 10B). For both assemblies, the PF decreases when the cuts are increased in the sinusoidal wave, reaching 25% for the 90% cuts, which means that only 1/4 of the available energy is used for the operation of the motor pump.

Figure 13 presents the variation in the power factor (PF) because of the change in hydraulic power for the different cuts made in the waveform. For both sets, high waveform cuts result in low hydraulic powers, but operating points within a range of high energy consumption are observed. Therefore, a direct relationship between the sinusoidal cut and the reduction in PF can be observed, meaning that it reduces the system's ability to use available energy in useful work.

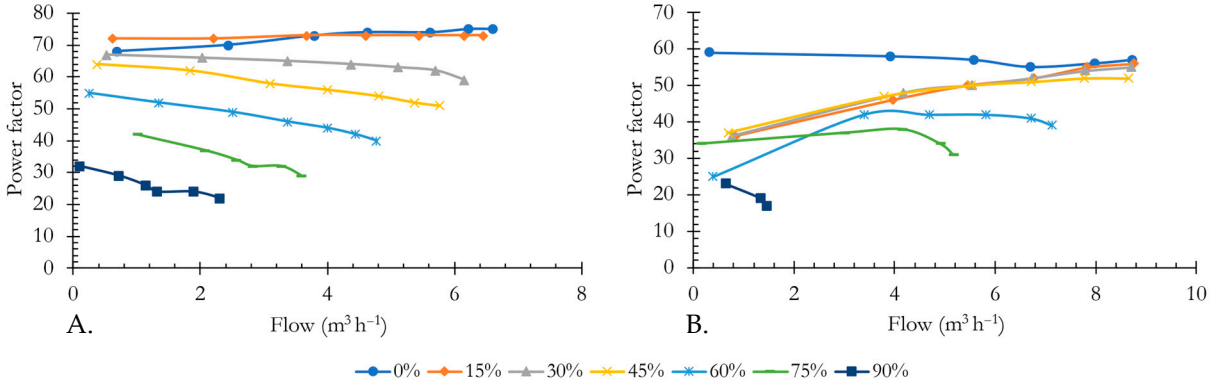

Figure 12. Power factor of the motor pumps as a function of flow rate for different percentage cuts in the sinusoidal waveform: (**A**) Pump A; (**B**) Pump B.

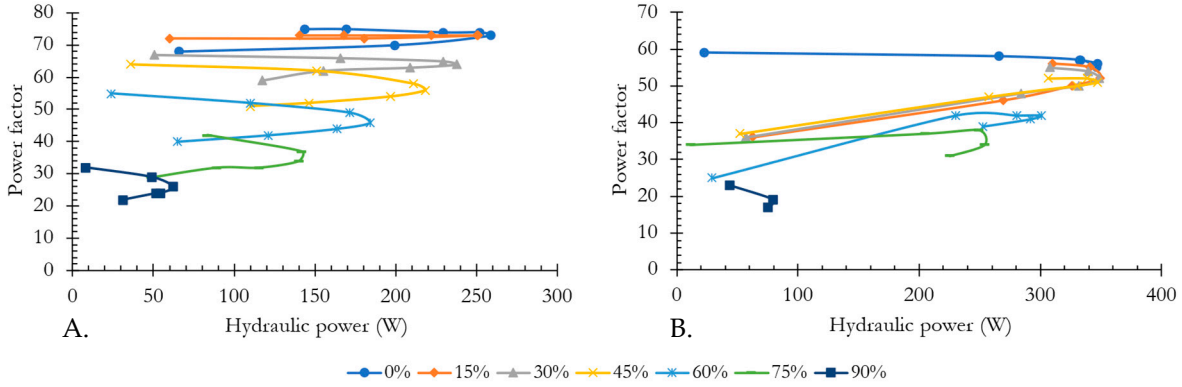

Figure 13. Power factor of the motor pumps as a function of hydraulic power for different percentage cuts of the sinusoidal waveform: (**A**) Pump A; (**B**) Pump B.

The total efficiency curves of the system as a function of flow rate and sinusoidal cuts are presented in Figure 14. It can be observed that pump B (Figure 14B) has twice the average efficiency compared to pump A (Figure 14A). Generally, there were no significant variations in efficiency when related to the waveform cut; however, cuts close to 90% showed an average reduction of 20% in efficiency for pump B and approximately 10% for pump A.

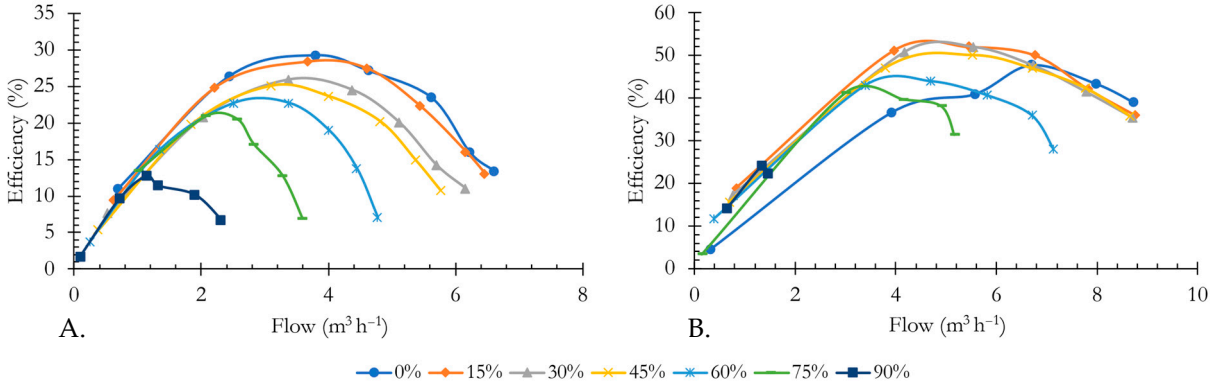

Figure 14. Curves of efficiency for different percentage cuts of the sinusoidal wave: (**A**) Pump A; (**B**) Pump B.

3.2. Characteristic Curves of Pumps and Range of Operations

The characteristic curves of the pumps used in the evaluation (flow vs. manometric head) are presented in Figure 15, both for operation without using the controller and for

the cuts made by the developed controller. For both pumps, the performance curves were altered when cuts were made in the sinusoidal wave, showing that this technique can help adjust the pump operating point according to the design point in pumping systems.

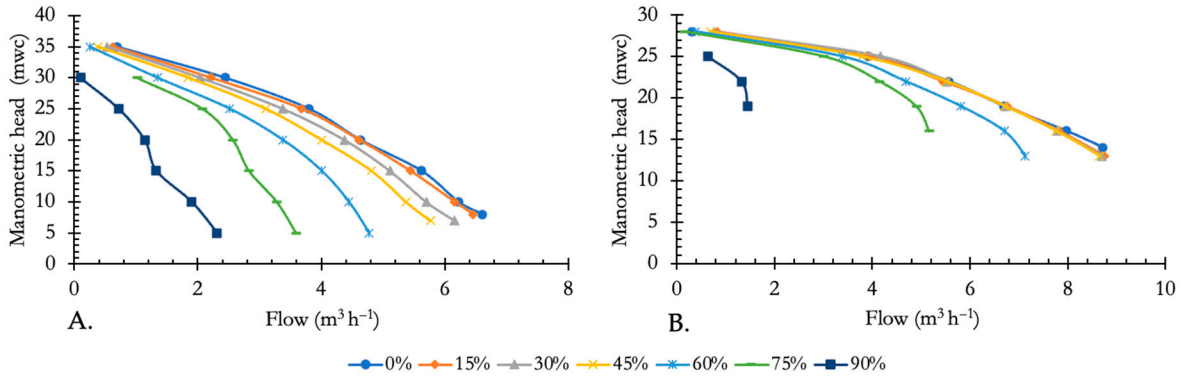

Figure 15. Characteristic curves of the pumps for different cuts of the sine wave (0; 15; 30; 45; 60; 75 and 90%) performed by the power controller. (**A**) Pump A; (**B**) Pump B.

The potential operating ranges of the units in response to wave cutting are presented in Figure 16. Using the controller, the pump acquires an operating area within its flow chart as a function of the head, instead of a single curve, allowing any combination within this region.

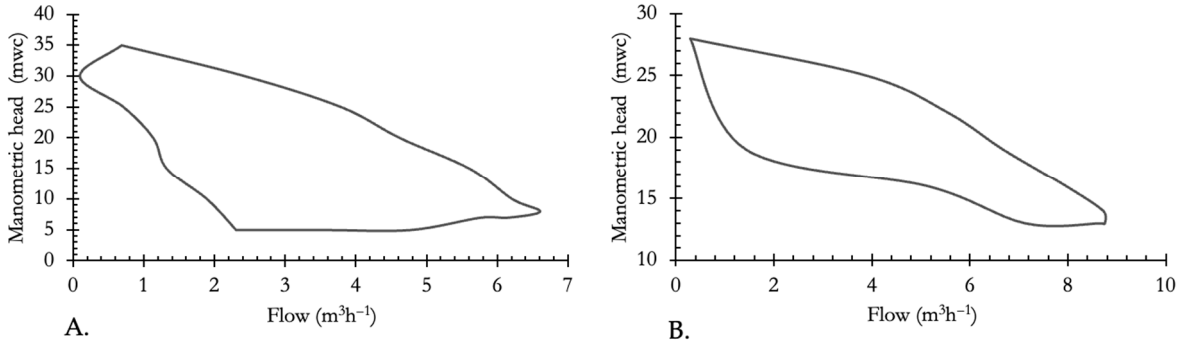

Figure 16. Useful operating range of the pump sets with the power controller: (**A**). Pump A; (**B**). Pump B.

3.3. Response Surface Methodology (RSM)

Figure 17 illustrates the response surface of the motor-pumps, depicting the correlation between the implemented firing angle control and the outlet pressure, and its resulting effect on the flow rate. It can be observed that higher flow rate ranges are achieved with lower firing angle control settings and reduced outlet pressures. Specifically, firing angle control settings up to 50% consistently yield higher outlet flow rates, accompanied by minimal associated pressure variations. This highlights a critical operating region where significant flow rates can be maintained without drastic pressure fluctuations, potentially indicating an efficient operating zone for the pump system. Furthermore, the fitted quadratic models for estimating the required firing angle control for various combinations of pressure and flow rate are presented in Equations (4) and (5), enabling precise predictive control of the system's operating point.

$$FAC = -25.9497 + 39.8398\,Q + 12.3285\,P - 1.8421\,QP - 4.9203\,Q^2 - 0.2918\,P^2 \quad (4)$$

$$FAC = -662.0431 + 111.5491\,Q + 62.8029\,P - 4.0896\,QP - 5.4915\,Q^2 - 1.3385\,P^2 \quad (5)$$

where

FAC—Firing Angle Control (%);
P—Pressure (mwc);
Q—Flow rate ($m^3\ s^{-1}$).

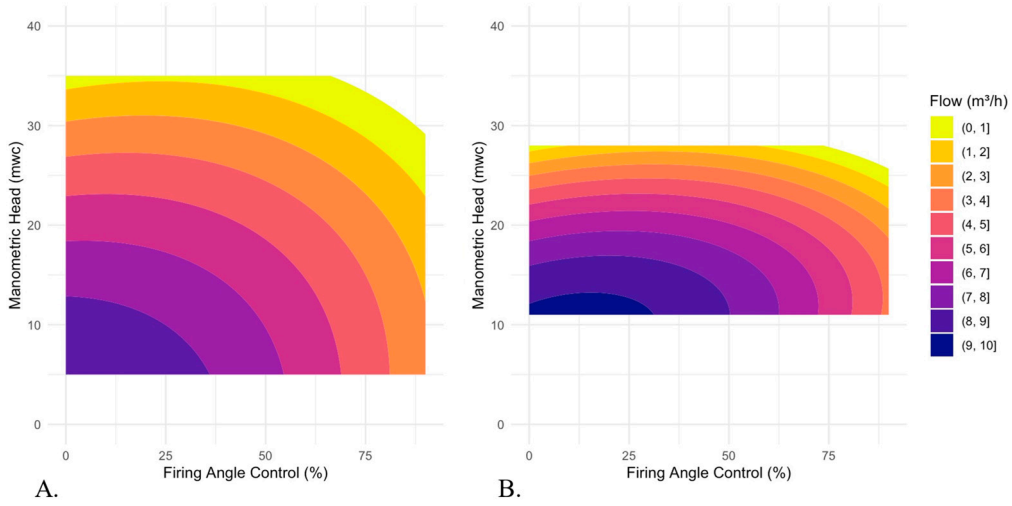

Figure 17. Interpolated response surface of the Flow Rate ($m^3\ h^{-1}$) as a function of the Firing Angle Control (%) and Pressure Head (mwc, meters of water column), based on the Response Surface Methodology (RSM): (**A**). Pump A; (**B**). Pump B.

Complementarily, Figure 18 presents the response surface of the motor-pumps, correlating the implemented firing angle control and hydraulic power, and illustrating the resulting variation in efficiency. An interesting inverse relationship can be observed between different operating regions on this surface concerning optimal performance: for certain conditions (e.g., 'for the first operating zone' or 'for a specific motor-pump set'), higher efficiencies are achieved at higher firing angle control settings and higher hydraulic powers. Conversely, for other conditions, optimal efficiencies are observed at higher hydraulic powers but with lower firing angle control settings. This divergence underscores the complex interplay between electrical control and hydraulic output, suggesting the existence of multiple optimal operating points or distinct control strategies depending on the desired performance parameters and the specific characteristics of the pump set. Furthermore, the fitted quadratic models for estimating efficiency, based on combinations of hydraulic power and the applied firing angle control, are detailed in Equations (6) and (7). These models provide a valuable tool for predicting the system's efficiency under various operational scenarios, aiding in the development of adaptive control strategies for energy optimization.

$$n_T = 6.8631 + 0.0542\ Pot_H - 0.2315\ FAC + 0.0008\ FAC\ Pot_H + 0.0001\ {Pot_H}^2 + 0.0021\ FAC^2 \quad (6)$$

$$n_T = 0.0854 + 0.2220\ Pot_H + 0.2312\ FAC - 0.0005\ FAC\ Pot_H - 0.0002\ {Pot_H}^2 - 0.0018\ FAC^2 \quad (7)$$

where

n_T—Total efficiency (%);
FAC—Firing Angle Control (%);
Pot_H—Hydraulic power (W).

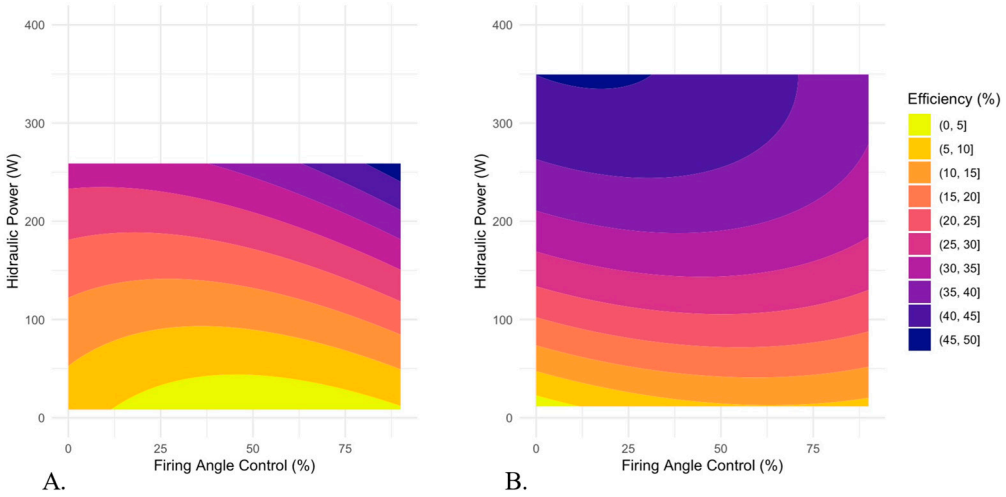

Figure 18. Interpolated response surface of the Efficiency (%) as a function of the Firing Angle Control (%) and Pressure Head (mwc, meters of water column), based on the Response Surface Methodology (RSM): Efficiency: (**A**) Pump A; (**B**) Pump B.

4. Discussion

4.1. Performance of Electric Motors Under Firing Angle Control

In general, the current consumption of Pump A (Figure 10A) increased proportionally to the waveform cut. In the 60 and 75% cuts, for flows above 4.5 and 3.0 m^3 h^{-1}, respectively, the consumed current exceeded 10 A, leading to overheating of the motor pump assembly. Pump B (Figure 10B) showed less proportionality between the waveform cut and current consumption, as the current versus flow curves were closer for different cuts. However, similarly to Pump A, in 60 and 75% cuts, for flows above 7 and 5 m^3 h^{-1}, respectively, the consumed current exceeded 10 A. It is noteworthy that motor heating occurs due to the overcurrent originating from the drop in the average supply voltage, which raises the temperature of the stator and motor winding above the insulation class. According to [30], the reduction in voltage can provide energy savings, which is greater with lower motor loads. However, voltage reduction results in increased currents and a maximum reduction limit must be set to avoid affecting motor performance.

It is important to highlight that this limitation is also present in other forms of speed control for single-phase AC motors, such as the use of frequency inverters. According to [7], when the frequency drops below 50% of the nominal frequency, the motor torque may be compromised, leading to increased slip and, consequently, higher electric current, which reduces motor efficiency.

Without cutting the supply sinusoidal, Pump A presented active power ranging from 600 to 1100 W (Figure 11A). Using the power controller, the lowest active power was 274 W for the 90% percentage cut. Pump B ranged from 500 to 800 W without waveform cutting and obtained active power values close to 182 W for the 90% cut (Figure 11B). It is noteworthy that the reduction in the active power of the motor-pump assemblies results in a reduction in energy consumption. Thus, in addition to adjusting the operating point, the controller allows a reduction in costs related to energy expenditure in the pumping process. According to [31], the speed control of single-phase motors through the TRIAC can provide considerable energy savings, in addition to simplicity, reliability and low acquisition cost.

According to [10], this reduction in the power factor, when speed control in single-phase motors is carried out based on TRIAC, is due to introducing voltage harmonics and an increase in stator current harmonics. According to the authors, in cases where torque is reduced, efficiency gains and loss reduction can be achieved. Otherwise, the introduction of harmonics by TRIAC-based speed control can lead to a reduction in motor

efficiency. According to [13,16], in addition to reducing efficiency, harmonics can increase torque pulsations in the motor, which can cause mechanical vibration [30] and acoustic noise. It also causes the stator temperature to rise, which can result in reduced motor life. Furthermore, they generate current and voltage distortions in the electrical network, which can affect the performance of other equipment [31]. Other forms of non-dissipative pressure control for irrigation systems, such as frequency inverters, also inject harmonics into the electrical network [32], making it recommended to use filters to mitigate their effect. According to [33] for drives less than 20 kW the harmonic contribution to the network is likely very small. Thus, the authors recommend that for loads between 20 and 400 kW, devices such as passive harmonic filter, active harmonic filter, or active front drive should be used, generating a significant improvement in the power factor.

4.2. Characteristic Curves of Pumps and Range of Operations

The operation of the two motor pumps regarding the variation in their operating point generated different responses, where Pump B presented less variation in the characteristic curves with the percentage cut of the sinusoidal wave. It is also worth noting that the curves obtained from the percentage cuts of the sinusoidal wave resemble the curves of pumps with smaller rotor diameters. It was observed that this effect was more effective for higher flow rates.

It is also worth mentioning that with a wider operating range, a single unit can meet the demand of several projects or even the variable demand of plots within the irrigated area, without needing to use hydraulic energy dissipating devices, such as pressure regulating valves, as recommended by [6]. Several studies have demonstrated the feasibility of using electrical or electronic devices to control pumping systems in center pivot irrigation systems [1,32], sprinkler irrigation [4] and water extraction from artesian wells [33]. The operating ranges found for the pump can be considered sufficient to meet most of the variation scenarios in manometric heights found in the field, considering the flow rate of maximum efficiency of the pump. For Pump A, a range of 7 to 32 mwc was obtained, while for Pump B it was 16 to 26 mwc. This corresponds to a reduction in the manometric head of 78% and 38%, respectively, for Pump A and Pump B. The variations in the manometric head found by [1,4,32] were, respectively, 41% for sprinkler irrigation, 50% and 38% for center pivot irrigation.

4.3. Response Surface Methodology

The optimization of energy efficiency in motor-pump systems, particularly within irrigation applications, represents a complex challenge driven by the imperative to reduce operational costs and promote sustainability [32,33]. The findings presented in Figures 17 and 18 offer valuable insights into the intricate interplay between the operating point control and the hydraulic and energetic performance of motor-pumps, leveraging Response Surface Methodology (RSM) to map these nonlinear relationships.

The observation that higher flow rate ranges are achieved with lower firing angle control settings and reduced outlet pressures (Figure 17) aligns well with the fundamental affinity laws for pumps, which predict a decrease in flow rate and head with a reduction in pump speed or supply voltage [4]. Crucially, the response surface analysis allows for the identification of specific regions of optimized operation. Notably, firing angle control settings up to 50% consistently yield significantly high outlet flow rates, accompanied by minimal associated pressure variations. This finding is pivotal for developing adaptive control strategies aimed at maximizing water delivery under specific demand conditions, while simultaneously managing system pressure efficiently [27].

The inherent complexity of the system is evident through the inverse relationship observed across distinct operational regions concerning optimal efficiency performance (Figure 18). While certain conditions demonstrate higher efficiencies at elevated firing angle control settings and increased hydraulic powers, other configurations exhibit optimal efficiencies at comparable high hydraulic powers but with notably lower firing angle control settings. This divergence in maximum efficiency points underscores the intricate nature of motor and pump efficiency curves, which are inherently nonlinear and highly dependent on the operating point [10,30]. The presence of multiple optimal points or high-efficiency zones highlights the need for dynamic control strategies capable of adapting the firing angle control in real-time to accommodate variations in flow rate and pressure demand, thereby ensuring the most energy-efficient operation.

The quadratic equations (Equations (4)–(7)) derived from the Response Surface Methodology (RSM) analysis serve as invaluable tools for estimating firing angle control and efficiency, respectively. These models facilitate the prediction of system behavior at unmeasured points and are fundamental for implementing predictive control systems. The ability to accurately forecast efficiency based on firing angle control and hydraulic power is particularly relevant for energy optimization, as it enables the control system to select the most efficient operating point for a given demand, directly contributing to the reduction in electrical energy consumption in irrigation pumping systems.

5. Conclusions

This study successfully designed, implemented, and evaluated a novel controller for regulating the operation of single-phase motor-pump sets commonly used in irrigation systems. The controller demonstrated robust performance, exhibiting no software or hardware malfunctions throughout the testing procedures. By precisely manipulating voltage through sine wave cuts, the controller effectively modulated power delivery to the motor, enabling accurate control of the pump's operating point. This capability facilitates optimized performance across a range of operational demands, enhancing the versatility and efficiency of the irrigation system.

A key feature of this controller is its user-friendly interface, achieved through seamless wireless communication and a dedicated smartphone application. This intuitive design allows for effortless control and monitoring of the motor-pump set, enhancing accessibility and usability for a wide spectrum of operators. The successful integration of wireless communication and a mobile application highlights the potential for remote operation and automation of irrigation systems, further contributing to improved water management practices.

A reduction in power factor was observed with the variation in pump set power, whereby the power factor reached values below 25% for the highest waveform cuts. Therefore, it is recommended to assess the economic feasibility of certain operating points to maximize the technical and economic benefits of the developed controller.

In conclusion, this research makes a significant contribution to the field of irrigation technology by introducing a robust and efficient controller for single-phase motor-pump sets. The successful implementation of this technology, characterized by its precise power modulation, intuitive interface, and demonstrated reliability, offers a compelling solution for optimizing irrigation practices and promoting responsible water resource management. By enabling precise control over water delivery and energy consumption, this innovation has the potential to revolutionize agricultural practices, leading to increased efficiency, reduced environmental impact, and ultimately, enhanced food security. Future research should delve deeper into the analysis of harmonic generation by the controller, quantifying the levels of total harmonic distortion and its direct impacts on the electrical grid and

motor performance. This investigation, utilizing power quality analyzers, would allow for the establishment of a precise correlation between the TRIAC firing angle, system efficiency, and motor thermal stress. Such data would be essential for the development of mitigation strategies and for enhancing the system's robustness in compliance with regulatory standards.

Author Contributions: Conceptualization, A.T.A., M.F.P., M.V.M.O., A.d.M.P. and D.F.d.C.; methodology, A.T.A., M.F.P., M.V.M.O., A.d.M.P. and D.F.d.C.; investigation, A.T.A. and M.F.P.; validation, A.T.A.; supervision, M.F.P., M.V.M.O., A.d.M.P. and D.F.d.C.; writing—original draft preparation, A.T.A., M.F.P., M.V.M.O., A.d.M.P. and D.F.d.C.; writing—review and editing, A.T.A. and M.F.P. All authors have read and agreed to the published version of the manuscript.

Funding: This research received no external funding.

Data Availability Statement: The data that support the findings of this study are available from the corresponding author, [A.T.A.], upon reasonable request.

Acknowledgments: We thank the Federal Rural University of Rio de Janeiro and institutions that funded the study.

Conflicts of Interest: The authors declare no conflicts of interest.

References

1. Brar, D.; Kranz, W.L.; Lo, T.; Irmak, S.; Martin, D.L. Energy Conservation Using Variable-Frequency Drives for Center-Pivot Irrigation: Standard Systems. *Trans. ASABE* **2017**, *60*, 95–106.
2. Khadra, R.; Moreno, M.A.; Awada, H.; Lamaddalena, N. Energy and Hydraulic Performance-Based Management of Large-Scale Pressurized Irrigation Systems. *Water Resour. Manag.* **2016**, *30*, 3493–3506. [CrossRef]
3. Lamaddalena, N.; Khila, S. Energy saving with variable speed pumps in on-demand irrigation systems. *Irrig. Sci.* **2012**, *30*, 157–166. [CrossRef]
4. de Araújo, J.A.B.; Seraphim, O.J.; Siqueira, J.A.C.; Presenço, F.; Caneppele, F.D.L. Avaliação de um sistema irrigação por aspersão com aplicação do inversor de freqüência no conjunto motobomba. *Irriga* **2006**, *11*, 319–327. [CrossRef]
5. Carvalho, J.d.A.; Mello, C.d.; Braga Júnior, R.A.; Reinato, C.H.; de Santana, M.J. Utilização do inversos de freqüência em sistemas de irrigação para controle de vazão. *Rev. Bras. De Eng. Agrícola E Ambient.* **2000**, *4*, 51–56. [CrossRef]
6. Pinto, M.F.; Pereira, D.J.d.S.; Carvalho, D.F.d.; Alves, D.G.; Salvador, C.A. Technical and economic feasibility of using a variable-frequency drive in micro-irrigation systems. *Eng. Agrícola* **2021**, *41*, 112–118. [CrossRef]
7. Collins, E.R. Torque and slip behavior of single-phase induction motors driven from variable frequency supplies. In Proceedings of the Conference Record of the 1990 IEEE Industry Applications Society Annual Meeting, Seattle, WA, USA, 7–12 October 1990; IEEE: New York, NY, USA, 1992; pp. 61–66.
8. Jannati, M.; Anbaran, S.A.; Asgari, S.H.; Goh, W.Y.; Monadi, A.; Aziz, M.J.A.; Idris, N.R.N. A review on Variable Speed Control techniques for efficient control of Single-Phase Induction Motors: Evolution, classification, comparison. *Renew. Sustain. Energy Rev.* **2017**, *75*, 1306–1319. [CrossRef]
9. Oliveira Filho, D.; Ferenc, C.H.R.; Teixeira, C.A.; Dias, G.P.; Milagres, R.C.; Pontes, C.R. Uso de motores monofásicos acoplados mecanicamente em série, em irrigação por pivô central. *Rev. Bras. De Eng. Agrícola E Ambient.* **2005**, *9*, 139–144. [CrossRef]
10. Mademlis, C.; Kioskeridis, I.; Theodoulidis, T. Optimization of Single-Phase Induction Motors—Part I: Maximum Energy Efficiency Control. *IEEE Trans. Energy Convers.* **2005**, *20*, 187–195. [CrossRef]
11. Williamson, S. Reduction of the Voltage and Current Harmonics Introduced by a Single-Phase Triac AC Controller, by Means of Shunt Resistance. *IEEE Trans. Ind. Electron. Control Instrum.* **1981**, *IECI-28*, 266–272. [CrossRef]
12. Valer, L.R.; Melendez, T.A.; Fedrizzi, M.C.; Zilles, R.; de Moraes, A.M. Variable-speed drives in photovoltaic pumping systems for irrigation in Brazil. *Sustain. Energy Technol. Assess.* **2016**, *15*, 20–26. [CrossRef]
13. Cunha, K.C.B.d.; Rocha, R.V.d. Automation in the irrigation process in family farming with Arduino 397 platform. *Rev. Eletrônica Competências Digit. Para. Agric. Fam.* **2016**, *1*, 62–74.
14. Alvarenga, A.C.; Ferreira, V.H.; Fortes, M.Z. Photovoltaic solar energy: An application in family 399 farming irrigation. *Sinergia* **2014**, *15*, 311–318.
15. Arif, Y.C.; Rakhmawati, R.; Saksana, A. Suhariningsih Implementation of AC-AC Voltage Controller for Reduce Transient Current at Three Phase Induction Motor. In Proceedings of the 2019 International Seminar on Application for Technology of Information and Communication (iSemantic), Semarang, Indonesia, 21–22 September 2019; IEEE: New York, NY, USA, 2019; pp. 465–470.

16. Lamaddalena, N.; Khila, S. Efficiency-driven pumping station regulation in on-demand irrigation systems. *Irrig. Sci.* **2013**, *31*, 395–410. [CrossRef]
17. Banik, A.; Umesh, J.; Bhadade, G.; Gaikwad, A. Speed Control of Single Phase Induction Motor using TRIAC and Bluetooth Device. In Proceedings of the 2023 IEEE 2nd International Conference on Industrial Electronics: Developments & Applications (ICIDeA), Imphal, India, 29–30 September 2023; IEEE: New York, NY, USA, 2023; pp. 516–521.
18. Kenly, W.L.; Bose, B.K. Triac Speed Control of Three-Phase Induction Motor with Phase-Locked Loop Regulation. *IEEE Trans. Ind. Appl.* **1976**, *IA-12*, 492–498. [CrossRef]
19. Sharma, U.; Singh, B. Investigations on TRIAC Based Speed Controller for a Single-Phase Induction Motor Ceiling Fans. In Proceedings of the 2021 International Conference on Sustainable Energy and Future Electric Transportation (SEFET), Hyderabad, India, 21–23 January 2021; IEEE: New York, NY, USA, 2021; pp. 1–6.
20. Di Gerlando, A.; Perini, R. Modelling and test validation of high speed universal motors fed via a triac. In Proceedings of the IEEE International Conference on Electric Machines and Drives, San Antonio, TX, USA, 15 May 2005; IEEE: New York, NY, USA, 2005; pp. 6–1178.
21. Islam, T.; Fayek, H.H.; Rusu, E.; Rahman, F. Triac Based Novel Single Phase Step-Down Cycloconverter with Reduced THDs for Variable Speed Applications. *Appl. Sci.* **2021**, *11*, 8688. [CrossRef]
22. Mathias, L.C.; Castanha, L.M.G.; de Oliveira, A.V.; Kuhn, E.V. Assessment of Phase Control and Time-Proportional Control Schemes for TRIAC Applications. *J. Control Autom. Electr. Syst.* **2023**, *34*, 1272–1283. [CrossRef]
23. KiCad Development Team. Available online: https://www.kicad.org/download/ (accessed on 10 September 2025).
24. ATMEL. Datasheet: ATmega48P/88P/168P/328P. Available online: https://www.alldatasheet.com/datasheet-pdf/pdf/194805/ATMEL/ATMEGA48P.html (accessed on 10 September 2025).
25. Texas Instruments. Datasheet: CC2541—2.4 GHz Bluetooth. 27–32. Available online: https://www.alldatasheet.com/datasheet-pdf/view/454131/TI/CC2541.html (accessed on 10 September 2025).
26. Palpankar, M.P.M. Induction Motor Speed Control by varying duty cycle of TRIAC. *J. Adv. Electr. Devices* **2018**, *3*, 23–28. [CrossRef]
27. Sungur, C.; Çalişir, S.; Kaya, E. Developing an Automation System for Improving the Energy Efficiency of Constant Pressure Irrigation Pumps. *J. Irrig. Drain. Eng.* **2016**, *142*, 04016052. [CrossRef]
28. Dean, A.; Voss, D.; Draguljić, D. Response Surface Methodology. In *Design and Analysis of Experiments*; Springer: New York, NY, USA, 2017; pp. 565–614.
29. R Core Team. *R: A Language and Environment for Statistical Computing*; R Foundation for Statistical Computing: Vienna, Austria, 2025.
30. Mohan, N. Improvement in Energy Efficiency of Induction Motors by Means of Voltage Control. *IEEE Trans. Power Appar. Syst.* **1980**, *PAS-99*, 1466–1471. [CrossRef]
31. Mademlis, C.; Theodoulidis, T.; Kioskeridis, I. Optimization of single-phase induction motors—Part II: Magnetic and torque performance under optimal control. *IEEE Trans. Energy Convers.* **2005**, *20*, 196–203. [CrossRef]
32. Moraes, M.J.; Oliveira Filho, D.; Mantovani, E.C.; Monteiro, P.M.B.; Mendes, A.L.C.; Damião, J.H.A.C. Automação em sistema de irrigação tipo pivô central para economia de energia elétrica. *Eng. Agrícola* **2014**, *34*, 1075–1088. [CrossRef]
33. Córcoles, J.I.; Gonzalez Perea, R.; Izquiel, A.; Moreno, M.Á. Decision Support System Tool to Reduce the Energy Consumption of Water Abstraction from Aquifers for Irrigation. *Water* **2019**, *11*, 323. [CrossRef]